Iron–Sulfur–Gold Clusters

Deutsche Ausgabe: DOI: 10.1002/ange.201504574
Internationale Ausgabe: DOI: 10.1002/anie.201504574

A Reduced 2Fe2S Cluster Probe of Sulfur–Hydrogen versus Sulfur–Gold Interactions

*Danielle J. Crouthers, Shengda Ding, Jason A. Denny, Ryan D. Bethel, Chung-Hung Hsieh, Michael B. Hall, and Marcetta Y. Darensbourg**

Abstract: *The Ph_3PAu^+ cation, renowned as an isolobal analogue of H^+, was found to serve as a proton surrogate and form a stable Au_2Fe_2 complex, $[(\mu\text{-}SAuPPh_3)_2\{Fe(CO)_3\}_2]$, analogous to the highly reactive dihydrosulfide $[(\mu\text{-}SH)_2\{Fe(CO)_3\}_2]$. Solid-state X-ray diffraction analysis found the two $SAuPPh_3$ and SH bridges in anti configurations. VT NMR studies, supported by DFT computations, confirmed substantial barriers of approximately 25 kcal mol^{-1} to intramolecular interconversion between the three stereoisomers of $[(\mu\text{-}SH)_2\{Fe(CO)_3\}_2]$. In contrast, the largely dative S–Au bond in $\mu\text{-}SAuPPh_3$ facilitates inversion at S and accounts for the facile equilibration of the $SAuPPh_3$ units, with an energy barrier half that of the SH analogue. The reactivity of the gold-protected sulfur atoms of $[(\mu\text{-}SAuPPh_3)_2\{Fe(CO)_3\}_2]$ was accessed by release of the gold ligand with a strong acid to generate the $[(\mu\text{-}SH)_2\{Fe(CO)_3\}_2]$ precursor of the [FeFe]H_2ase-active-site biomimetic $[(\mu_2\text{-}SCH_2(NR)CH_2S)\{Fe(CO)_3\}_2]$.*

Transition-metal sulfide clusters are presumed to have played an important role in energy metabolism even before the proliferation of life on planet Earth and before the paleoatmosphere became enriched in oxygen. An appealing hypothesis is that in the presence of CO the simplest of iron–sulfur clusters, Fe_2S_2, developed and detached as molecular $[(\mu\text{-}S_2)\{Fe(CO)_3\}_2]$, or possibly its hydrogenated form, $[(\mu\text{-}HS)_2\{Fe(CO)_3\}_2]$, from a precursor mineral surface, such as iron pyrite (Figure 1).[1] These complexes could therefore be early abiotic analogues of the diiron hydrogenase ([FeFe]-H_2ase) active site (Figure 1), to be later replaced by biosynthetic paths required for protection of the organism from the toxic diatomic ligands in the [FeFe]H_2ase active site. In fact, $[(\mu\text{-}S_2)\{Fe(CO)_3\}_2]$ enjoys current fame as the synthetic precursor to a host of small molecules that are biomimetic analogues of the active site of [FeFe]H_2ase, thus connecting the inorganic to the biological world, through organometallic chemistry (Figure 1).

Studies of SH^- as a ligand are of importance to the bioinorganic chemistry of iron; however, examples and studies of isolated Fe–SH units are sparse.[2] Discrete hydrosulfido complexes can be synthesized through protonation of sulfido ligands, an example of which is the protonation of the reduced, anionic sulfido-bridged species $[(\mu\text{-}S)_2\{Fe(CO)_3\}_2]^{2-}$ to form $[(\mu\text{-}SH)_2\{Fe(CO)_3\}_2]$.[3] Although the spectroscopic signatures (ν(CO) and NMR spectra) of $[(\mu\text{-}SH)_2\{Fe(CO)_3\}_2]$ have been known for decades, its X-ray crystal structure has not been reported until now.

Because of the well-known isolobal analogy between Ph_3PAu^+ and H^+, the former may serve as a surrogate for the latter, thus leading to experimental strategies particularly useful in the structural determination of many organometallic compounds containing transition-metal hydrides.[4] The Ph_3PAu^+ unit has also been used to model the protonation of metal-bound thiolates, with the generation of thiolate-bridged $M(\mu\text{-}SR)Au^I$ moieties.[5] Herein we report the isolation of $[(\mu\text{-}SAuPPh_3)_2\{Fe(CO)_3\}_2]$ and $[(\mu\text{-}SH)_2\{Fe(CO)_3\}_2]$, and their characterization by X-ray diffraction. The spectroscopic properties and chemical reactivity of these two complexes as well as the nickelated complex $[(\mu_3\text{-}S)_2Ni(dppe)\{Fe(CO)_3\}_2]$ (dppe = 1,2-bis(diphenylphosphanyl)-ethane) were compared.[6] Interestingly, the stable polymetallic complexes can be used as synthons for $[(\mu\text{-}SCH_2N(R)CH_2S)\{Fe(CO)_3\}_2]$ through the intermediacy of the highly unstable HS analogue; the azadithiolate is a necessary cofactor for the 2Fe subsite of [FeFe]H_2ase.[7]

Reduction of the disulfide bond of $[(\mu\text{-}S_2)\{Fe(CO)_3\}_2]$ by $LiEt_3BH$ (2 equiv) in THF at −78 °C produces the $[(\mu\text{-}S)_2\{Fe(CO)_3\}_2]^{2-}$ dianion, whose versatility has been amply demonstrated by the preparation of myriad diiron complexes containing features of the [FeFe]H_2ase active site.[8] Protonation of the dianion with trifluoroacetic acid (2 equiv) by the method of Seyferth and co-workers yielded $(\mu\text{-}SH)_2[\{Fe(CO)_3\}_2]$ (**1**) and shifted the ν(CO) bands of the dianion by approximately + 50 cm^{-1}, as expected for the formation of the neutral SH derivative.[3] The product **1** was an air-sensitive red solid with similar ν(CO) values to those of its persulfide precursor, $[(\mu\text{-}S_2)\{Fe(CO)_3\}_2]$ (see Figure S1 in the Supporting Information).

Complex **2**, $[(\mu\text{-}SAuPPh_3)_2\{Fe(CO)_3\}_2]$, the desired analogue of **1**, was isolated as a thermally and air stable red solid upon the addition of $[Ph_3PAuCl]$ (2 equiv) to $[(\mu\text{-}S)_2\{Fe(CO)_3\}_2]^{2-}$. The ν(CO) values in the IR spectrum of **2** show a shift from those of the dianion by only about + 10 cm^{-1} (see Figure S1); that is, there is an approximately 40 cm^{-1} difference as compared to **1**. This result implies more negative charge in the 2Fe core of **2**, as seen in other S-bridged polymetallic diiron complexes, such as $[(\mu_3\text{-}S)_2Ni(dppe)\{Fe(CO)_3\}_2]$ (prepared by the addition of $[(dppe)NiCl_2]$ to $[(\mu$-

[*] D. J. Crouthers, S. Ding, J. A. Denny, Dr. R. D. Bethel, Prof. M. B. Hall, Prof. M. Y. Darensbourg
Department of Chemistry, Texas A&M University
College Station, TX 77843 (USA)
E-mail: marcetta@chem.tamu.edu
Dr. C.-H. Hsieh
Department of Chemistry, Tamkang University
New Taipei City 25157 (Taiwan)

Supporting information for this article is available on the WWW under http://dx.doi.org/10.1002/anie.201504574.

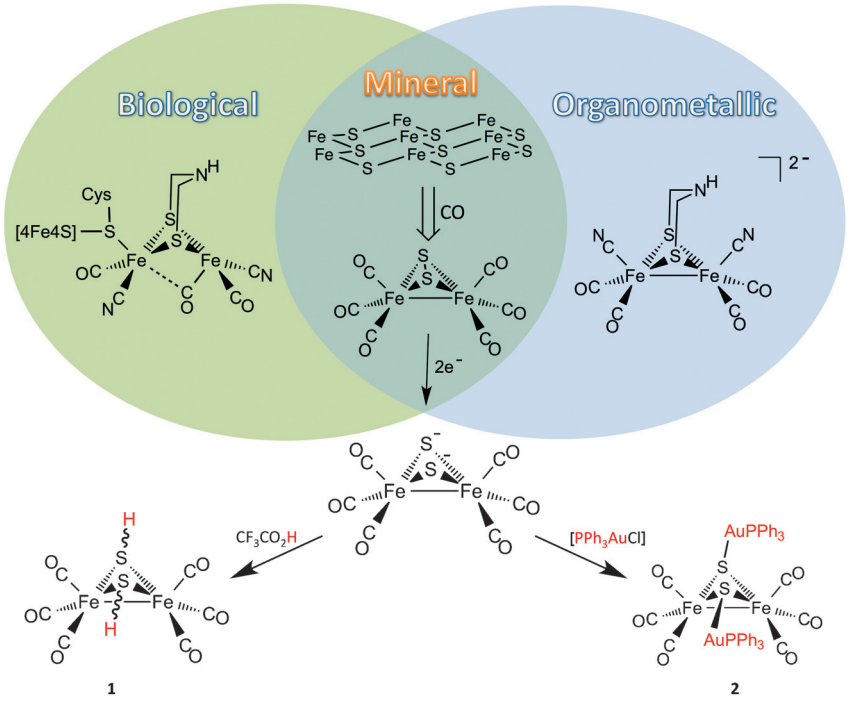

Figure 1. Diagram of the biological [FeFe] hydrogenase active site and the organometallic active-site model of [FeFe] hydrogenase. The two structures are connected through the possible primordial precursor $[(\mu\text{-}S_2)\{Fe(CO)_3\}_2]$.[1] Current biomimetic syntheses utilize the reduced form of the persulfide.

S)$_2${Fe(CO)$_3$}$_2$]$^{2-}$).[6] This known complex is included in the following reactivity section as a comparison or baseline for the sulfur–metal interaction.

Complexes **1** and **2** were crystallized from concentrated solutions in hexanes and THF, respectively, by slow cooling. The molecular structures of complexes **1** and **2** (Figure 2) were determined by X-ray diffraction analysis, and refined to R_1 factors of 3.17 and 3.76%, respectively. Complex **1** co-crystallized with the starting material, $[(\mu\text{-}S)_2\{Fe(CO)_3\}_2]$, in a 93:7 ratio. According to the areas of maximum electron density, the hydrogen atoms on the thiolate groups in complex **1** were found in the *anti* configuration positions, in analogy with the gold atoms in **2**. The $Fe_2(CO)_6$ units in **1** and **2** are almost superimposable (see Figure S2). (The other possible orientational isomers, syn_{ax} and syn_{eq}, would have both substituents oriented upwards, or both outwards, with respect to the 2Fe2S core.)

The Au–Au distance of 5.19 Å within complex **2** is beyond that expected for intramolecular aurophilic interactions, as most occur at a distance of about 3 Å.[9] Likewise, the shortest intermolecular Au–Au distance is 7.81 Å (see Figure S9). The geometry about the gold atoms is nearly linear (∡S-Au-P = 172.9 and 176.3°). The Fe_{avg}-S-Au angles are 115.4° for the equatorial gold atom and 104.9° for the axial gold atom; these angles differ slightly from those of complex **1**, with ∡Fe_{avg}-S-H_{eq} = 103.4° and ∡Fe_{avg}-S-H_{ax} = 107.7°.

Whereas the average Au–S bond distance in **2** is 2.315 Å, the observed distance between the axial gold atom and the sulfur atom bonded to the equatorial gold atom within the *anti* isomer is 3.041(2) Å, that is, shorter than the sum of the van der Waals radii of 3.24 Å. Space-filling models indicate the overlap and presumed interaction (see Figure S12). This likely interaction between the axial gold atom and the adjacent sulfur atom is interpreted as an explanation for the lack of a syn_{eq} isomer of **2**.

The ^{1}H NMR spectrum of $[(\mu\text{-}SH)_2\{Fe(CO)_3\}_2]$ in solution in $CDCl_3$ at 22°C displays four resonances, previously assigned to three isomers (syn_{ax}-**1**, syn_{eq}-**1**, and *anti*-**1**; Figure 4).[3] Only two isomers are observed for $[(\mu\text{-}SR)_2\{Fe(CO)_3\}_2]$ (R = Me, Et, and Ph). They have been isolated and separated by chromatography, and identified as *anti* and syn_{eq}, present in an approximately 4:1 ratio.[10,11] In these cases, the absence of the syn_{ax} isomer is ascribed to steric encumbrance, which is overcome in the linked thiolates $[(\mu\text{-edt})\{Fe(CO)_3\}_2]$ (edt = ethanedithiolate) and $[(\mu\text{-pdt})\{Fe(CO)_3\}_2]$ (pdt = propanedithiolate), and which is minimal in **1**. In contrast, the ^{31}P NMR spectrum of complex **2** in $CDCl_3$ at 22°C is a single broad resonance at 34.8 ppm, suggestive of ongoing exchange processes.

The dependence of the isomer ratio on temperature in complexes **1** and **2** was examined by ^{1}H and ^{31}P NMR spectroscopy. The four ^{1}H resonances observed at room temperature for complex **1** occur in ratios that differ slightly according to the solvent; however, the *anti* isomer always predominates. In C_6D_6, the *anti*/syn_{eq}/syn_{ax} ratio of 12:5:4 was maintained upon warming to 70°C, with no evidence of signal

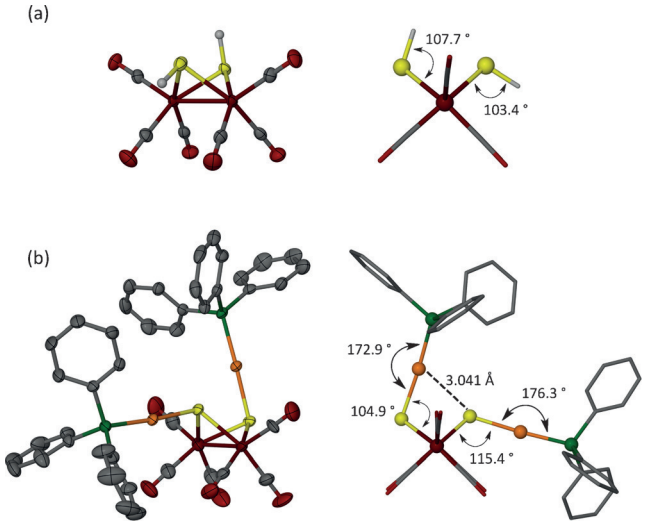

Figure 2. Molecular structures of complexes a) **1** and b) **2**. Left: Side view of thermal ellipsoids drawn at the 50% probability level. Right: View along the iron–iron bond in ball-and-stick models. Average Fe-S-Au angles are given.

broadening. This result is consistent with descriptions of the [(μ-SMe)$_2${Fe(CO)$_3$}$_2$] derivative.[11] From the ratios in C_6D_6, the thermodynamic stability of *anti*-**1** exceeds that of *syn*$_{ax}$-**1** and *syn*$_{eq}$-**1** by −0.67 and −0.56 kcal mol^{-1}, respectively.

The ^{31}P NMR spectrum of complex **2** displayed two sharp signals at 36.6 and 35.4 ppm at −60 °C in a ratio of approximately 1:1, and a small signal at 37.6 ppm (Figure 3).

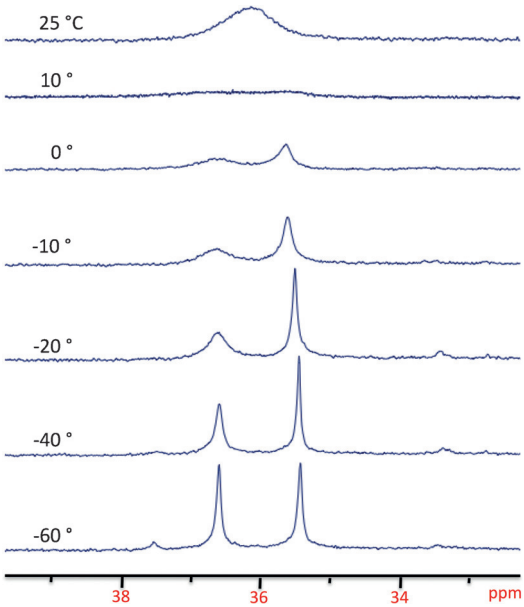

Figure 3. Variable-temperature ^{31}P NMR spectra at 121.4 MHz in [D$_8$]toluene for complex **2.**

The two major signals, assigned to non-equivalent P nuclei in *anti*-**2**, broadened and coalesced between 0 and 10 °C. Above this temperature, a single resonance appeared at 36.4 ppm for the equilibrated phosphorus nuclei. The experimental barrier for this exchange was calculated from the peak separation and coalescence temperature to be 13.3 kcal mol^{-1}.[12] The line widths of the two major signals are solvent- and temperature-dependent (Figure 3; see also Figures S15 and S16). Efforts to simulate the unequal broadening of the two major peaks in the experiment, including the assignment of the small peak mentioned previously to the P atoms of *syn*$_{eq}$-**2**, are described in the Supporting Information.

According to a review by Toyota,[13] multiple mechanisms are possible for the inversion of pyramidal sulfur. Mueting and Mattson measured an E_{act} barrier of 29.0 kcal mol^{-1} for the isomerization between the *syn*$_{eq}$ and *anti* isomers of [(μ-SMe)$_2${Fe(CO)$_3$}$_2$] and concluded that Fe–S bond rupture and reformation occurred during the isomerization.[14] From recent computational studies for the same system, Lichtenberger and co-workers found that a simple inversion at sulfur could account for the lowest-energy pathway (E_{act} = 26.8 kcal mol^{-1}).[15] Such barriers are high enough to prevent rapid exchange at ambient temperature.

Density functional theory (DFT) computations were performed to calculate the Gibbs free energy of each isomer of **1** and **2** as well as the activation energy barrier for conversion between the isomers. As described above, the small steric encumbrance of the SH unit, and an apparent high barrier to inversion at S, permits the observation of all three isomers of **1** by ^{1}H NMR spectroscopy. DFT calculations, with thermal and solvation corrections, found similar Gibbs free energies (*G*) for these isomers, whereby the *syn*$_{ax}$-**1** and *syn*$_{eq}$-**1** isomers were less stable than *anti*-**1** by 1.4 and 0.5 kcal mol^{-1}, respectively (Figure 4). This result is qualitatively consistent with the experimental ratios determined by the NMR studies, in which the major product was found to be the *anti* isomer, followed by the *syn*$_{eq}$ and *syn*$_{ax}$ isomers (see above). As for **2**, the calculations indicated that *syn*$_{eq}$-**2** is slightly less stable than *anti*-**2** by 0.7 kcal mol^{-1}, whereas *syn*$_{ax}$-**2** is less stable by 10.6 kcal mol^{-1} (Figure 4). The high energy of *syn*$_{ax}$-**2** is attributable to the steric repulsion between the two bulky triphenylphosphine ligands, even though they were found (by computation) to interdigitate to minimize the repulsion (see Figure S17).

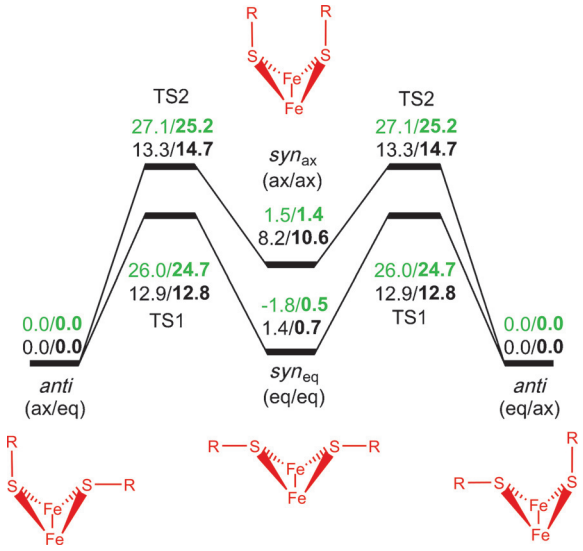

Figure 4. Energy profile of the transitions between the three isomers of **1** (in green) and **2** (in black, to which the profile is scaled). The calculated electronic energies, E_{ele}, in a vacuum are shown in light face, whereas the Gibbs free energies, *G*, after thermal and solvation corrections are shown in bold face (solvent: benzene for **1** and toluene for **2**).

As reported by Lichenberger and co-workers for the [(μ-SMe)$_2${Fe(CO)$_3$}$_2$] complex,[15] our calculations for the interconversion of isomers of complexes **1** and **2** found for both a transition-state structure with a pseudo-trigonal-planar sulfur moiety, HSFe$_2$ or AuSFe$_2$ (see Figure S18). The activation energy barriers between the *anti* and the two *syn* isomers of **1** were calculated to be 24.7 (TS1-**1**, between *anti*-**1** and *syn*$_{ax}$-**1**) and 25.2 kcal mol^{-1} (TS2-**1**, between *anti*-**1** and *syn*$_{eq}$-**1**), whereas the transition states (TSs) for **2** are much more accessible, with Gibbs free energy barriers of 12.8 (TS1-**2**) and 14.7 kcal mol^{-1} (TS2-**2**), in agreement with the experimental observations. The intermediate, *syn*$_{eq}$ or *syn*$_{ax}$, of the exchange process of **2**, as reflected by ^{31}P NMR spectroscopy, depends on the order of the motions of the two

moieties, via TS1 and TS2, respectively (Figure 4). The route featuring TS1, with a lower barrier, is slightly favored over the alternative route via TS2. The most accessible path for **2** qualitatively fits the experimental value, 13.3 kcal mol^{-1}. Because of the 1.9 kcal mol^{-1} difference between TS1 and TS2, the lifetime of P_{ax} of *anti*-**2** is only approximately 1/30 of that of P_{eq}. Thus, the ^{31}P signal of P_{ax} is expected to broaden prior to that of P_{eq} as the temperature is raised. Therefore, the two signals at 36.6 and 35.4 ppm for **2** at low temperature can be assigned to the P_{ax} and P_{eq} atoms of *anti*-**2**, respectively. Other mechanistic trials for the conformation exchange in **2**, which involved the dissociation–association of PPh_3 or $AuPPh_3^+$, or concerted semaphore-like motions of both $AuPPh_3$ units, did not yield an acceptable route with a relatively low barrier.

The high barriers (TS1 and TS2) of **1** are due to the electronic reorganization required for inversion of a pyramidal sulfur atom to access the trigonal-planar, sp^2-type bonding from bonds that were largely of the p^3 type.[13,16] However, despite its analogy to the proton, the gold–phosphine moiety in **2** is able to lower the planar barrier because it does not require the S atom to significantly rehybridize during the inversion. This interpretation is reflected by metric data and NBO analysis (see Tables S3 and S4 in the Supporting Information). In the inversion TSs (TS1-**2** and TS2-**2**), the two Fe–S bonds continue to utilize mainly p contribution from the S atoms for bonding, whereas the Au dative bond to S changes readily from accepting the S 3p lone pair in the pyramidal ground state to accepting the 3s lone pair in the planar transition states (see Table S4). In conclusion, the gold perturbs the electronic structure of the Fe_2S moiety less in the motion to the transition states, and those transition states have low energies in turn.

Many studies have shown that carbonyl-ligand substitution, by cyanide or phosphines, takes place readily with alkylated sulfur derivatives, such as $[(\mu\text{-SMe})_2\{Fe(CO)_3\}_2]$ and especially $[(\mu\text{-pdt})\{Fe(CO)_3\}_2]$.[17] Complex **1** undergoes similar PR_3/CO exchange under anaerobic conditions; however, when exposed to air, the product of PR_3 substitution immediately oxidizes to the disulfide, $[(\mu\text{-}S_2)\{Fe(CO)_3\}\{Fe(CO)_2(PR_3)\}]$.[18] In contrast, CO substitution by PPh_3 or $P(OMe)_3$ in complex **2** and $[(\mu_3\text{-}S)_2Ni(dppe)\{Fe(CO)_3\}_2]$ only proceeds in low yields. Decomposition occurs on addition of the strongly donating phosphine PMe_3, presumably because the $[AuPPh_3]^+$ or $[(dppe)Ni]^{2+}$ moiety is pulled out by PMe_3, concomitant with the release of $[(\mu\text{-}S)_2\{Fe(CO)_3\}_2]^{2-}$, which is unstable at room temperature. We conclude that the iron atoms in **2** and in $[(\mu_3\text{-}S)_2Ni(dppe)\{Fe(CO)_3\}_2]$ are more electron rich than those in **1** because the dative S–Au and S–Ni bonds are less capable of removing negative charge from the sulfide. As a result of these differences, the CO substitution on **2** is made more difficult than on **1**, in which the negative charge on the sulfide is neutralized well by a proton through a covalent bond.

To determine if the polymetallic, Fe_2Ni or Fe_2Au_2, complexes could be synthons for the azadithiolate derivative $[(\mu_2\text{-}SCH_2(NR)CH_2S)\{Fe(CO)_3\}_2]$, we explored conditions that would favor the formaldehyde/amine condensation reaction. Whereas direct addition was not successful, either with **2** or with the $[(\mu_3\text{-}S)_2Ni(dppe)\{Fe(CO)_3\}_2]$ complex, the addition of a strong acid, HCl or HBF_4, to complex **2** and then treatment with CH_2O and NH_2R, either in a one-pot reaction or following the isolation of intermediate **1**, readily yielded the azadithiolate (Figure 5).

In summary, the $[(\mu\text{-}SAuPPh_3)_2\{Fe(CO)_3\}_2]$ complex, as an isolobal analogue of $[(\mu\text{-}SH)_2\{Fe(CO)_3\}_2]$ and a molecular mimic of an aurolated or metalated FeS surface, was synthesized and crystallized (with the large $AuPPh_3$ units found in the solid state in the *anti* orientation), as was the hydrosulfido diiron complex. Solution NMR spectroscopic studies of the latter found all possible isomers, *anti*, syn_{ax}, and syn_{eq}. The small calculated differences in Gibbs free energy are consistent with the experimental distribution of the three isomers at room temperature and reflect a high barrier to isomerization owing to substantial electronic reorganization at sulfur in the transition states. In contrast, the dative character of the $Fe_2S^- \rightarrow AuPPh_3^+$ bond enables such sulfur inversion to occur with less perturbation of electronic structure. Through selective sulfur protonation with a strong acid, with release of the exogeneous metal, the polymetallic complexes $[(\mu\text{-}SAuPPh_3)_2\{Fe(CO)_3\}_2]$ and $[(\mu_3\text{-}S)_2Ni(dppe)\{Fe(CO)_3\}_2]$ were converted into azadithiolate derivatives through an amine/aldehyde condensation reaction. Hence, the S-centers in the metalated ion–sulfur species are protected from reactivity, in a manner similar to organic protecting agents. Such inorganic protecting agents for sulfur may also have significance for the hypothesis expressed earlier regarding the abiotic origin of the diiron hydrogenase active site.

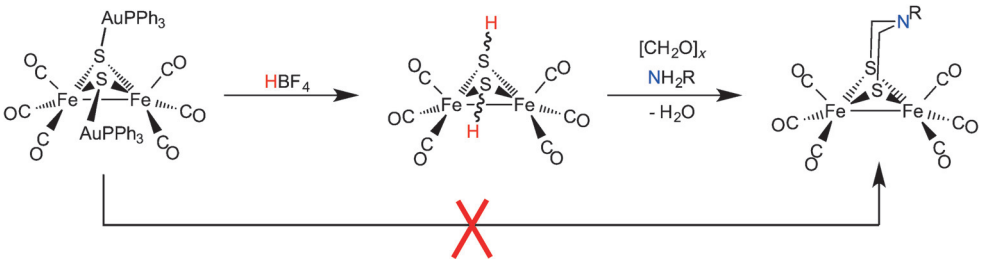

Figure 5. Synthesis of $[(\mu\text{-}SCH_2NRCH_2S)\{Fe(CO)_3\}_2]$ through the release of gold from $[(\mu\text{-}PPh_3AuS)_2\{Fe(CO)_3\}_2]$, with complex **1** as an intermediate. The direct condensation of formaldehyde and primary amines with **2** was not observed.

Acknowledgements

The experimental work was made possible by an NPRP award (NPRP 6-1184-1-224) from the Qatar National Research

Fund (a member of Qatar Foundation). The statements made herein are solely the responsibility of the authors. We also recognize the National Science Foundation (CHE-1266097 to M.Y.D., CHE-1300787 to M.B.H) and the Robert A. Welch Foundation (A-0924 to M.Y.D., A-0648 to M.B.H), especially for funding of the computational studies.

Keywords: hydrogenases · hydrosulfides · iron–sulfur–gold clusters · isolobal species · sulfur inversion

How to cite: *Angew. Chem. Int. Ed.* **2015**, *54*, 11102–11106
Angew. Chem. **2015**, *127*, 11254–11258

[1] a) G. Wächtershäuser, *Prog. Biophys. Mol. Biol.* **1992**, *58*, 85–201; b) G. Wächtershäuser, *Philos. Trans. R. Soc. London Ser. B* **2006**, *361*, 1787–1808; c) G. D. Cody, N. Z. Boctor, T. R. Filley, R. M. Hazen, J. H. Scott, A. Sharma, H. S. Yoder, *Science* **2000**, *289*, 1337–1340; d) S. E. McGlynn, D. W. Mulder, E. M. Shepard, J. B. Broderick, J. W. Peters, *Dalton Trans.* **2009**, 4274–4285.

[2] a) S. Kuwata, M. Hidai, *Coord. Chem. Rev.* **2001**, *213*, 211–305; b) C.-C. Tsou, W.-C. Chiu, C.-H. Ke, J.-C. Tsai, Y.-M. Wang, M.-H. Chiang, W.-F. Liaw, *J. Am. Chem. Soc.* **2014**, *136*, 9424–9433.

[3] a) D. Seyferth, R. S. Henderson, *J. Organomet. Chem.* **1981**, *218*, C34–C36; b) D. Seyferth, G. B. Womack, R. S. Henderson, *Organometallics* **1986**, *5*, 1568–1575.

[4] a) F. G. A. Stone, *Angew. Chem. Int. Ed. Engl.* **1984**, *23*, 89–99; *Angew. Chem.* **1984**, *96*, 85–96; b) H. G. Raubenheimer, H. Schmidbaur, *Organometallics* **2012**, *31*, 2507–2522; c) R. Hoffmann, *Angew. Chem. Int. Ed. Engl.* **1982**, *21*, 711–724; *Angew. Chem.* **1982**, *94*, 725–739; d) D. G. Evans, D. M. P. Mingos, *J. Organomet. Chem.* **1982**, *232*, 171–191.

[5] a) E. Fritsch, K. Polborn, C. Robl, K. Suenkel, W. Beck, *Z. Anorg. Allg. Chem.* **1993**, *619*, 2050–2060; b) J. Ruiz, V. Rodríguez, C. Vicente, J. M. Martí, G. López, *Inorg. Chem.* **2001**, *40*, 5354–5360.

[6] a) D. Seyferth, R. S. Henderson, L.-C. Song, *Organometallics* **1982**, *1*, 4899–4909; b) L.-C. Song, X.-J. Sun, G.-J. Jia, M.-M. Wang, H.-B. Song, *J. Organomet. Chem.* **2014**, *761*, 10–19.

[7] J. Esselborn, C. Lambertz, A. Adamska-Venkatesh, T. Simmons, G. Berggren, J. Noth, J. Siebel, A. Hemschemeier, V. Artero, E. Reijerse, M. Fontecave, W. Lubitz, T. Happe, *Nat. Chem. Biol.* **2013**, *9*, 607–609.

[8] a) C. Tard, C. J. Pickett, *Chem. Rev.* **2009**, *109*, 2245–2274; b) H. Li, T. B. Rauchfuss, *J. Am. Chem. Soc.* **2002**, *124*, 726–727; c) M. Y. Darensbourg, E. J. Lyon, J. J. Smee, *Coord. Chem. Rev.* **2000**, *206–207*, 533–561.

[9] H. Schmidbaur, A. Schier, *Chem. Soc. Rev.* **2012**, *41*, 370–412.

[10] a) B. King, M. B. Bisnette, *Inorg. Chem.* **1965**, *4*, 1663–1665; b) R. B. King, *J. Am. Chem. Soc.* **1962**, *84*, 2460.

[11] a) L. Maresca, F. Greggio, G. Sbrignadello, G. Bor, *Inorg. Chim. Acta* **1971**, *5*, 667–674; b) R. D. Adams, F. A. Cotton, W. R. Cullen, D. L. Hunter, L. Mihichuk, *Inorg. Chem.* **1975**, *14*, 1395–1399.

[12] H. Kessler, *Angew. Chem. Int. Ed. Engl.* **1970**, *9*, 219–235; *Angew. Chem.* **1970**, *82*, 237–253.

[13] S. Toyota, *Rev. Heteroatom. Chem.* **1999**, *21*, 139–162.

[14] A. Mueting, M. Mattson, *J. Inorg. Nucl. Chem.* **1981**, *43*, 749–751.

[15] O. In-noi, K. J. Haller, G. B. Hall, W. P. Brezinski, J. M. Marx, T. Sakamoto, D. H. Evans, R. S. Glass, D. L. Lichtenberger, *Organometallics* **2014**, *33*, 5009–5019.

[16] M. B. Hall, *Inorg. Chem.* **1978**, *17*, 2261.

[17] a) F. Gloaguen, J. D. Lawrence, M. Schmidt, S. R. Wilson, T. B. Rauchfuss, *J. Am. Chem. Soc.* **2001**, *123*, 12518–12527; b) B. Li, T. Liu, M. L. Singleton, M. Y. Darensbourg, *Inorg. Chem.* **2009**, *48*, 8393–8403; c) F. Gloaguen, T. B. Rauchfuss, *Chem. Soc. Rev.* **2009**, *38*, 100–108.

[18] L.-C. Song, P.-H. Zhao, Z.-Q. Du, M.-Y. Tang, Q.-M. Hu, *Organometallics* **2010**, *29*, 5751–5753.

Received: May 20, 2015
Published online: July 31, 2015

